

Ferromagnetic resonance in the epitaxial system Fe/MgO/Fe with coupled magnetic layersE. Popova,* C. Tiusan, and A. Schuhl
*LPM, CNRS–Université H. Poincaré, 54506 Vandoeuvre-lès-Nancy, France*F. Gendron
*INSP, Université P. et M. Curie, 75015 Paris, France*N. A. Lesnik
Institute of Magnetism of National Academy of Science of Ukraine, 03142 Kyiv, Ukraine
(Received 2 June 2006; revised manuscript received 24 October 2006; published 14 December 2006)

Temperature and thickness dependencies of ferromagnetic resonance (FMR) characteristics, such as resonance field, signal intensity, and linewidth have been studied at 9.25 GHz in both tunnel junctions MgO(100)/Fe1/MgO/Fe2/V and in single iron films MgO(100)/Fe/V having the same growth parameters as in junctions. The FMR data have been interpreted on the basis of structural and static magnetic measurements performed in this work, and compared with the known model of FMR in ultrathin magnetic layers coupled through a nonmagnetic spacer. An exponential decay of the coupling strength with spacer layers thickness together with the decrease of the coupling under film cooling found by the FMR, are in good agreement with the Slonczewski and Bruno theories developed for free electron spin polarized tunneling between the ferromagnetic layers across an insulating barrier.

DOI: [10.1103/PhysRevB.74.224415](https://doi.org/10.1103/PhysRevB.74.224415)

PACS number(s): 76.50.+g, 73.40.Rw

I. INTRODUCTION

Since the 1960s, a periodic revival of scientific interest in magnetic multilayers is closely related to recurrent developments in the field of functional electronics and computer facilities. For the last few years an interest in magnetic multilayers has grown even more,¹ since a very high tunneling magnetoresistance (TMR) ratio was expected to be obtained in epitaxial magnetic tunnel junctions (MTJ) containing two magnetic layers separated by an insulating MgO barrier. Such systems have been studied recently (e.g., in Refs. 2–8). Although the measured TMR ratios were large,^{2,3} they did not reach predicted values. A plausible reason of this discrepancy is believed to be due to the oxidation of Fe layer at the Fe/MgO interfaces.⁵

A theory describing the conductance of tunnel junctions has been developed by Slonczewski,⁹ who has interpreted experiments by Gittleman¹⁰ and Jullière¹¹ on the basis of band theory and proposed a model for the interlayer coupling (IC) through a tunneling barrier at $T=0$. The important role of the interfacial structure in the magnetoresistance (MR) effect has been shown. According to recent studies,^{12–15} the tunnel transmission becomes strongly affected by resonant effects at the interfaces. The signature of the interfacial resonance in the tunneling has been demonstrated in Fe1/MgO/Fe2/V films with the thin MgO spacer by conductivity measurements.¹⁶ In Refs. 6 and 7 we studied advanced MTJs containing a Co layer, that is, Fe1/MgO/Fe2/Co/V. The spacer thickness range, for which the coupling is antiferromagnetic, has been determined from room temperature static magnetic measurements. On the one hand, an exponential IC decay with growing spacer thickness established by magnetometric measurements, indicates a spin-polarized quantum tunneling to be the main mechanism of the interlayer exchange interaction in these systems. On the other hand, AF coupling has been

found for the spacer thickness range lying well below the smallest thickness limit of the MgO layer estimated for this coupling type in Ref. 17 using the Slonczewski model.⁹ Further studying of the coupling mechanism requires temperature measurements. In the framework of the spin-polarized quantum tunneling theory the interlayer coupling should increase with temperature, contrary to the predictions of the other models, e.g., the model of the impurity assisted exchange coupling having a resonant origin.¹⁷ It should be noted, that the analysis of the temperature dependence of the magnetometry data of IC faces difficulties because of the strong temperature dependence of the anisotropy energy. Ferromagnetic resonance (FMR), as seen below, is a more suitable technique for such investigations.

In the current paper we interpret X-band FMR spectra observed in the trilayer junctions Fe1/MgO/Fe2/V (V is the capping layer) that exhibit an interlayer exchange. In this case the analysis of the data is more reliable due to the simplified film structure compared to the structure of the advanced MTJ system with cobalt Fe1/MgO/Fe2/Co/V. IC effects are deduced by studying thickness and temperature dependencies of the resonance fields, as well as of the FMR signal intensity and linewidth both in trilayers and in single layer Fe reference samples deposited under similar conditions. An interpretation of the FMR spectra of the films is based on the data of our structural and magnetometric measurements and on the theoretical descriptions of FMR in coupled magnetic layers.^{18,19}

II. SAMPLE PREPARATION AND CHARACTERIZATION

Epitaxial Fe1/MgO/Fe2 structures of different layer thicknesses were deposited using the molecular-beam epitaxy (MBE) technique. Iron layers were prepared by thermal

evaporation from a standard Knudsen cell. A 10 nm thick V capping layers, as well as MgO spacer layers, were prepared by means of an electron gun. The first Fe layer was deposited on an annealed MgO substrate that had the cubic axes parallel with the specimen edges. It was annealed for 15 min at 450 °C and then a MgO insulating layer, having a thickness of 0.6, 0.8, or 1.0 nm, was subsequently deposited. Then the second Fe layer was epitaxially grown on the top of the MgO barrier. The thickness of the first Fe layer varied in the range of 10–34 nm, the thickness of the second one was in the range 3.5–30 nm and its determination error was within ± 5 –7 % of the layer thickness. The MgO thickness values have been measured using the reflection high energy electron diffraction (RHEED) technique. Clear RHEED intensity oscillations were observed allowing a determination of the MgO layer thickness (d^{MgO}) with a low absolute uncertainty: less than ± 0.05 nm. The films consisted of high quality ultrathin layers without pinholes and had flat interfaces. The continuity of the insulating layer has been previously checked down to 0.5 nm using transmission electron microscopy (TEM), electrical, and magnetoresistance measurements. The growth conditions and the characterization of the films have been described in more details in Refs. 6 and 7.

The crystalline structure of the samples was determined using TEM and x-ray diffraction measurements. The iron layer grew pseudomorphically on the MgO(100) substrate, but the Fe unit cell was rotated by 45° with respect to the MgO unit cell. The epitaxial relationship was: Fe(100)[110]||MgO(100)[100]. The annealed layers were found to be single crystalline. The structure of the second iron layer grown on the top of the insulating barrier was similar to the structure of the first layer. This layer was not annealed as its surface was quite smooth without any evidence of polycrystallinity or texture. In the trilayers the iron cells were rotated by 45° with respect to the MgO unit cells similar to case of single iron layers deposited onto MgO substrates. The films exhibited two hard magnetic axes [110] parallel to the sample edges and two easy axes [100]_{Fe} in the plane (100)_{Fe} oriented parallel to the diagonals of the square sample.

The magnetization curves have been investigated by means of a superconducting quantum interference device (SQUID) and alternating gradient field magnetometers. Magnetization versus magnetic field loops have been obtained on multilayer films with lateral sizes greater than a few millimeters. A magneto-optical Kerr rotation setup was used to measure the hysteresis loop of the thinnest ($d^{\text{Fe}}=3.5$ nm) single Fe layer. Due to the epitaxial growth, both Fe layers present fourfold symmetry and have an easy/hard axis in the top layer parallel to that in the bottom layer.

FMR experiments have been performed using an X-band VARIAN spectrometer operating at the frequency $f \approx 9.25$ GHz in the field range (–100–2500) mT. The power of the microwave field \mathbf{h} , directed in most cases parallel to the sample surface, was 1 mW. A sample holder was mounted at the center of the resonance cavity within the rf magnetic component antinode allowing both the in-plane and out-of-plane rotation of the sample with respect to the static

applied magnetic field. The angular dependencies of the resonance field $\mathbf{H}_r(\theta, \varphi)$ were measured in the films having different thicknesses of the top iron layer $d^{\text{Fe}2}$ or of the insulating barrier d^{MgO} . The angle θ between the direction of the applied magnetic field \mathbf{H} and the film normal \mathbf{n} was varied from $\theta=90^\circ$ (\mathbf{H} was in the film plane, $\mathbf{H} \perp \mathbf{n}$) to $\theta=0$ ($\mathbf{H} \parallel \mathbf{n}$). The angle φ characterizing the in-plane rotation was measured from the direction of the in-plane hard axis of the magnetocrystalline anisotropy, the iron [110] axis. In this case \mathbf{h} was directed perpendicular to the film surface.

The general condition of the ferromagnetic resonance is²¹

$$\left(\frac{\omega}{\gamma}\right)^2 = \frac{1}{M^2 \sin^2 \theta_M} [F_{\theta_M \theta_M} F_{\varphi_M \varphi_M} - F_{\theta_M \varphi_M}^2], \quad (1)$$

where $\omega=2\pi f$, and γ is the gyromagnetic ratio. θ_M and φ_M are equilibrium polar and azimuthal angles of the magnetization \mathbf{M} in the spherical coordinate system. They can be found from the equations of equilibrium

$$F_\theta \equiv \frac{\partial F}{\partial \theta} = 0; \quad F_\varphi \equiv \frac{\partial F}{\partial \varphi} = 0. \quad (2)$$

The free energy density F includes the Zeeman contribution, as well as the shape, magnetocrystalline and uniaxial anisotropy energies. If the specimen consists of coupled layers, the magnetic coupling energy should also be taken into account. The FMR equations and their analysis in the case of the epitaxial single (001) – oriented Fe film are reported, for instance, in Refs. 22 and for the films with coupled layers the analysis is performed in Refs. 18 and 19.

III. EXPERIMENT AND DISCUSSION

We investigate: (i) single Fe layers deposited on the MgO substrates and capped with a 10 nm thick V layer (MgO/Fe_x/V₁₀) to simulate the Fe₂ layers in the stack Fe1/MgO/Fe2/V, (ii) the stack itself, and (iii) the Fe film on the MgO substrate covered with the MgO and V layers (MgO/Fe₃₄/MgO_{1.5}/V₁₀) in order to simulate the boundary conditions for the first iron layer in the complete MTJ. The Fe single-layer thicknesses of 3.5, 6.5, 11, 34 nm, are close to the Fe thicknesses in the trilayers. Subscripts indicate the corresponding layer thicknesses in nm.

A. Room temperature FMR and SQUID data in single iron films Fe/V

The structural and magnetic properties of thin epitaxial iron films have been well studied, e.g., in Refs. 5, 20, 22, and 25. In this section we show that the properties of our Fe specimens are similar to those reported in the literature. The good quality of the investigated layers allows a better analysis of the magnetic coupling mechanism in the studied MTJs.

According to Prinz *et al.*,²⁰ magnetic properties of the ultrathin ($d^{\text{Fe}} \leq 5.0$ nm, the exchange length in Fe at room temperature¹⁸) MBE grown Fe films are surface dominated. The partial oxidation of iron and the occurrence of a strained FeO layer at the MgO/Fe interfaces⁵ may cause a modification of magnetic parameters in the local interfacial regions.

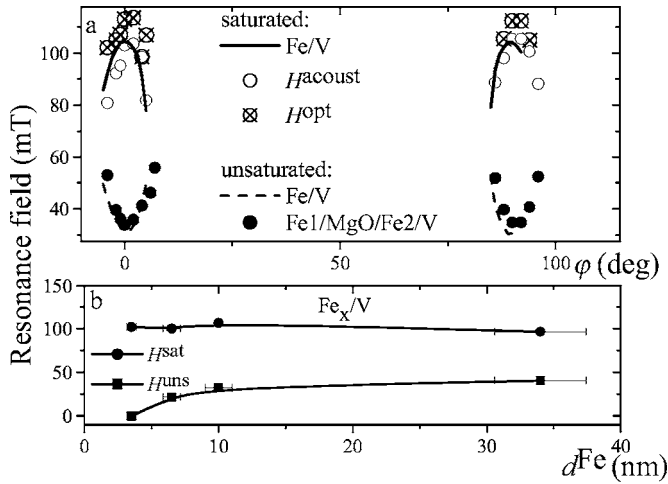


FIG. 1. Angular ϕ dependencies of the resonance field (a) in saturation (solid lines) and nonsaturation (dashed lines) regimes in the representative $\text{Fe}_{34}/\text{MgO}/\text{V}_{10}$ film and in the $\text{Fe}_{30}/\text{MgO}_{0.8}/\text{Fe}_{20}/\text{V}_{10}$ stack: open circles correspond to the acoustic mode, crossed circles belong to the optical mode, solid circles indicate unsaturated resonance. The angle ϕ is measured from the hard axis. Thickness dependencies of the parallel resonance fields in single iron films (b): solid circles indicate resonance fields under saturation; data below saturation are shown by solid squares. The layer thicknesses in nm are shown by subscripts. The measurements have been performed at $f=9.25$ GHz and $T=300$ K. Angular ϕ dependencies of the resonance field indicate fourfold in-plane symmetry.

Generally, the ultrathin Fe films grown on MgO substrates exhibit two surface uniaxial anisotropies. According to Ref. 18, the perpendicular anisotropy originates from a vertical lattice distortion because of a horizontal “film-substrate” structural mismatch. This would give rise to a twofold anisotropy $E=-K \cos^2 \theta$ and thus an effective magnetization (M_{eff}) described in Ref. 22. The parallel uniaxial anisotropy occurs in films with vicinal surfaces or having unidirectional interface chemical ordering (e.g., Ref. 18 and references therein). It was not found in our samples.

The FMR spectra in iron films consist of two well separated lines. Double peaks of this type have been earlier observed and interpreted in monocrystalline nickel ferrite.²¹ It has been shown (e.g., Refs. 20–22) that in a single iron layer the appearance of two resonance peaks is due to the strong magnetocrystalline anisotropy field H_A . The high field signal is the conventional saturated resonance, meanwhile the low field peak occurs below saturation as a result of a precession of the film magnetization \vec{M} at the effective field $\vec{H} < H_A$. The anisotropy is also responsible for a disappearance of both resonance peaks when the applied field deviates from the anisotropy hard axis. We observed that effect in Fe films, as shown in Fig. 1(a) by the solid (saturation regime) and dashed (nonsaturation regime) lines. The two signals have been detected in all samples in a wide temperature range (1.4–300 K). In this work the FMR study of the samples is mainly focused on the FMR in saturated films.

The upper curve in Fig. 1(b) demonstrates that the thickness dependence of H_r^{sat} in the Fe series is weak. This is

consistent with weak magnetic surface energy pinning, or its absence, and justifies a simple model, in which the thick iron films are treated like the ultrathin layers having the uniform magnetization.²⁶ As shown in Ref. 22, at the in-plane dc magnetic field the Fe film can be treated in such a way up to the thickness of 100 nm.

The values of both the saturation magnetization, $M_s \cong 1700$ G, determined by SQUID, and the FMR resonance field in our specimens are close to the values known from the literature for iron films with similar crystalline structure and thickness, e.g., in Ref. 22 and references therein. Unfortunately, an absence of the signal at 9 GHz, when the samples were magnetized along an easy axis, did not allow us to determine the energy of the fourfold anisotropy. However, the H_A value has been found²² to be close enough to the value for bulk iron. Our measurements give for the perpendicular resonance field $H_r^\perp = 2314$ mT. Using the simple equation for the perpendicular FMR configuration^{18,26}

$$\left(\frac{\omega}{\gamma}\right) = H_r^\perp - 4\pi M_{\text{eff}} + H_A, \quad (3)$$

and assuming both $H_A = 56$ mT (the bulk value) and the spectroscopic factor $g=2.09$ (e.g., Refs. 18 and 22), we estimate $4\pi M_{\text{eff}}$ at 20.5 kG; $4\pi M_{\text{eff}} = 4\pi M_s - H_u$. Here $H_u \approx 85$ mT is the uniaxial anisotropy field due to the vertical lattice distortion and broken symmetry at the interface.²²

B. Room temperature FMR and SQUID data in Fe1/MgO/Fe2/V junctions

Representative FMR spectra in junctions $\text{Fe1}/\text{MgO}/\text{Fe2}/\text{V}$ at fixed thicknesses of both the first Fe layer ($d^{\text{Fe1}}=30$ nm) and the insulating barrier ($d^{\text{MgO}}=0.6$ nm), are shown in Figs. 2(a)–2(c). The saturated signals are observed to the right of the dashed line.

In accordance with a theoretical model^{18,19} describing the FMR in coupled ultrathin layers, the two high field resonance peaks are acoustic and optical modes. The layer magnetizations precess in a coupled manner that results in an acoustic mode (when the magnetic moments in the two layers are in phase) and in an optical mode (when they rotate in antiphase). In the cited works the exchange coupling between the magnetic layers 1 and 2 is taken in the form

$$E_{\text{ex}} = -J_{12} \frac{\vec{M}_1 \cdot \vec{M}_2}{M_1 M_2}, \quad (4)$$

where J_{12} is the coupling parameter and \vec{M}_1, \vec{M}_2 are the magnetizations of the layers 1 and 2.

The angular dependencies of the resonance fields $H_r(\theta)$ in the representative samples (Fig. 3) show that the optical mode is observed at higher fields than the acoustic one, that is better seen for the film shown in the inset. Hence the coupling is antiferromagnetic in agreement with Refs. 18 and 19. The value of $4\pi M_{\text{eff}}$ estimated using the θ dependence of the resonance field for the $\text{Fe}_{30}/\text{MgO}_{0.6}/\text{Fe}_{20}/\text{V}_{10}$ film, is approximately 21 kG. We used values of K_1 and g obtained for the single Fe films (see above) and $H_r^\perp = 2360$ mT. In the thinner sample having $d^{\text{Fe2}}=10$ nm (see the inset) H_r^\perp

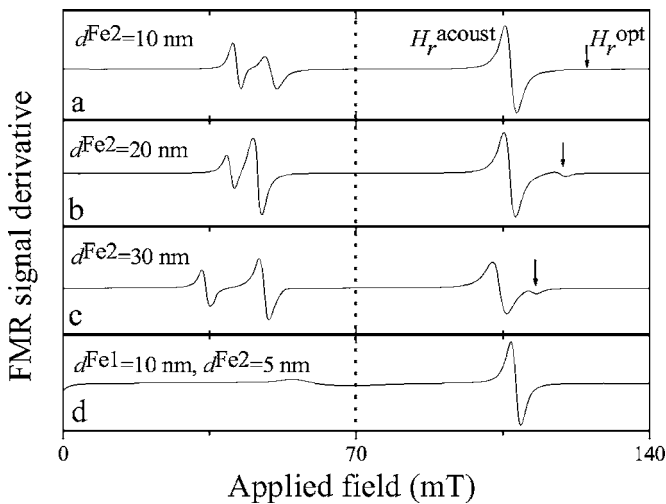


FIG. 2. In-plane FMR spectra in the Fe1/MgO/Fe2/V films with different $d^{\text{Fe}2}$: 10 nm (a); 20 nm (b); 30 nm (c); 5 nm (d). Layer thicknesses are: $d^{\text{MgO}}=0.6$ nm; $d^{\text{Fe}1}=30$ nm (a)-(c), and 10 nm (d). Unsaturated and saturated resonances are respectively on the left and on the right of the dashed line. Positions of the optical mode are indicated by arrows. The FMR spectra were recorded at $f=9.25$ GHz in the film plane along the hard magnetic axis. $T=300$ K.

≈ 2500 mT. This is at the upper bound of the applied field range and cannot be accurately measured.

The FMR signals in trilayers are observed in the vicinity of the hard anisotropy axis ($\varphi=90^\circ$) only, as it can be seen from the angular φ dependencies of the resonance fields shown in Fig. 1(a). These plots for the stack (symbols) are similar to those for the single iron film (lines). Note that in the $\text{Fe}_{30}/\text{MgO}_{0.8}/\text{Fe}_{20}/\text{V}_{10}$ film [Fig. 1(a)], the coupling is not strong, that is $H_{\text{ex}} < 5$ mT.

Hysteresis loops measured at 300 K in junctions $\text{Fe}1/\text{MgO}_x/\text{Fe}2/\text{V}$, having different thicknesses (x) of insu-

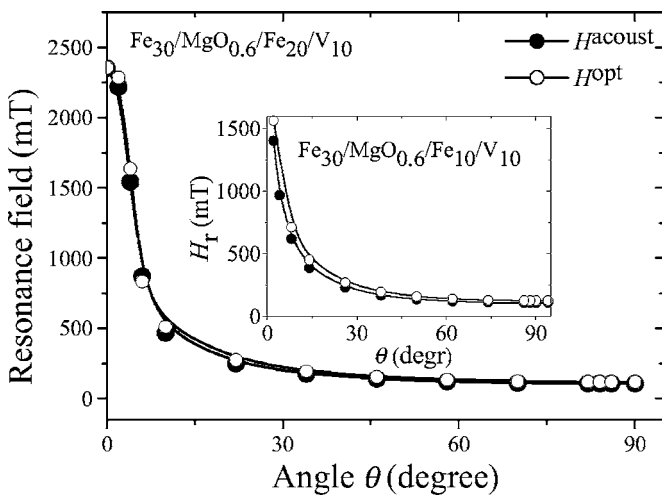


FIG. 3. Room temperature angular θ dependencies of the resonance fields H_r^{acoust} (solid circles) and H_r^{opt} (open circles) in the stacks $\text{Fe}1/\text{MgO}/\text{Fe}2/\text{V}$ with different thicknesses of the top Fe layer: 10 nm (inset) and 20 nm. At $\theta=90^\circ$ magnetic field H is applied along a hard magnetization axis.

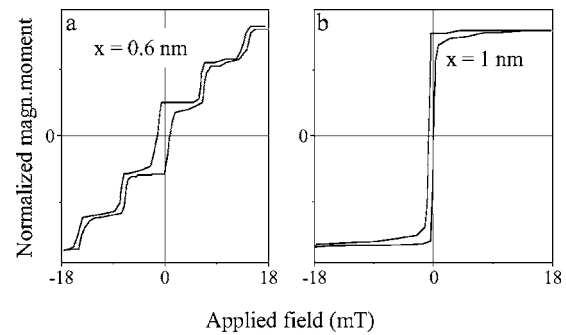


FIG. 4. Hysteresis loops in the $\text{Fe}_{30}/\text{MgO}_x/\text{Fe}_{20}/\text{V}_{10}$ films depending on the thickness x of MgO spacer. $x=0.6$ nm (a), 1.0 nm (b). The field was applied in the film plane along an easy magnetization axis. $T=300$ K.

lating layers, are shown in Fig. 4. An asymmetry of the minor loops (not shown here), which decreases with growing d^{MgO} , and the presence of steps [Fig. 4(a)] indicate an antiferromagnetic coupling, in agreement with the FMR data. If the field is applied along one easy axis, the second easy axis is perpendicular to the field. This explains the two-step reversal observed between 10 and 20 mT. Indeed, when the magnetization of the thinner magnetic layer reverses towards the antiparallel configuration, it will be trapped in the anisotropy quantum well related to the second easy axis.

The values of the interlayer exchange fields H_{ex} were determined from the minor hysteresis loops. Figure 5 shows the experimental dependence $H_{\text{ex}}(d^{\text{MgO}})$ manifesting an exponential decrease of the exchange coupling with the spacer thickness in agreement with the Slonczewski's theory. However, the linear dependence of the coupling field on the inverse thickness of the Fe layer, shown in the inset, cannot follow from this model, in which a simple case of the interface coupling between semi-infinite electrodes is considered.

In the FMR experiments a measure of the coupling strength is the difference between the resonance fields of the

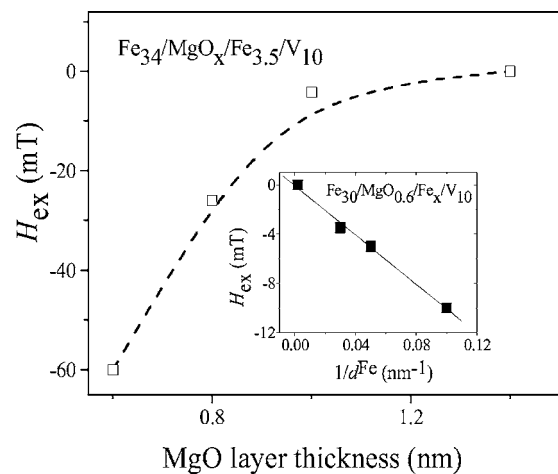


FIG. 5. The MgO thickness dependencies of the exchange field in $\text{Fe}1/\text{MgO}/\text{Fe}2/\text{V}$ stacks at 300 K, determined from magnetization measurements. The open squares indicate experimental values of H_{ex} . The line is exponential fit. The exchange field depending on the inverse thickness of the top Fe layer is shown in the inset.

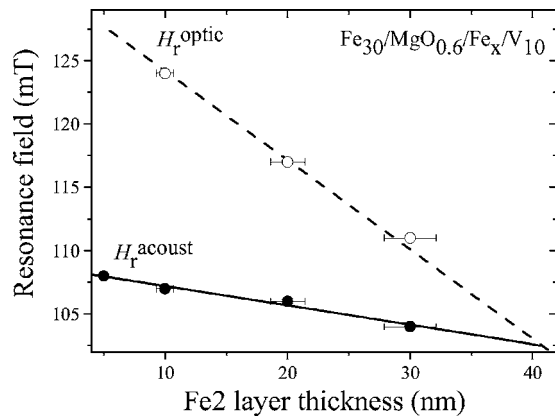


FIG. 6. Acoustic and optical in-plane resonance fields versus Fe2 layer thickness in the $\text{Fe}_{30}/\text{MgO}_{0.6}/\text{Fe}_x/\text{V}_{10}$ films at 300 K.

optical and acoustic modes: $\delta H_r = H_r^{\text{optic}} - H_r^{\text{acoust}}$.

Figures 2 and 6 show dependencies of the optical and acoustic resonance fields on the top iron layer thickness at the fixed thicknesses of the bottom iron layer and the MgO spacer. The stronger is the coupling, the larger is δH_r . The acoustic peak moves to lower fields with growing $d^{\text{Fe}2}$, meanwhile the optical resonant signal approaches the acoustic one and its intensity increases [Figs. 2(a)–2(c)]. Such a behavior of the signals is evidence of the weakening of antiferromagnetic coupling.^{18,19} As distinct from these plots, the trilayer having thinner Fe layers demonstrates a single resonance [Fig. 2(d)], therefore the strong IC. The presence of some pinholes in the MgO layer in this case cannot be fully excluded. Reverting to Fig. 2(c), note that the optical mode is observed at the equal nominal thicknesses of both Fe layers, though in this case only the acoustic resonance can be present. But, in fact, an error on the d^{Fe} value runs up to 7%.

The graphs in Fig. 6 clearly show that the coupling between the Fe layers depends on their thickness. It decreases with increasing thickness of the top Fe layer and is not detectable anymore at $d^{\text{Fe}2} > 40$ nm. Note that a simple model describing two iron films with uniform magnetizations coupled by a surface exchange energy term, does not predict a linear dependence of the optical resonance field on iron layer thickness. Therefore in that case the form (4) of the exchange coupling may not be quite correct.

A decrease of the coupling (shown by the decrease of δH_r) is also observed if the spacer thickness is increased (Fig. 7). It is clearly seen, that at equal spacer thicknesses the interlayer coupling is stronger in ultrathin multilayers (open circles). In this figure the experimental thickness dependence of the exchange field (open squares) obtained by SQUID in the same ultrathin film, is shown for a comparison. The FMR and SQUID data are in good agreement.

C. Temperature dependence of FMR parameters

Temperature measurements have been performed to further verify the validity of the Bruno's model²³ for the interlayer coupling in the Fe/MgO/Fe system. In this theory an expression for the coupling constant reduces to Slonczewski's result at $T=0$. Data obtained using SQUID do not give a

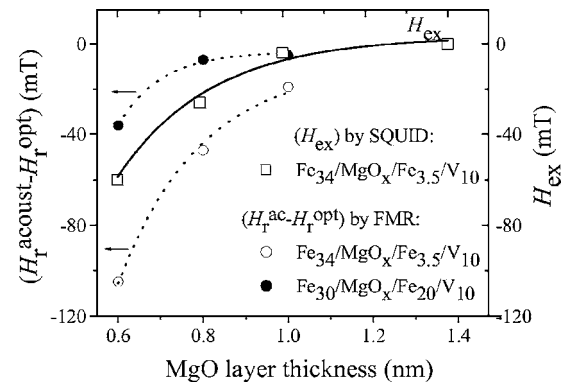


FIG. 7. The separation between parallel resonance fields of acoustic and optical modes as a function of the MgO spacer thickness in two samples $\text{Fe}1/\text{MgO}/\text{Fe}2/\text{V}$ differing by the Fe2 layer thickness: 3.5 nm (open circles) and 20 nm (solid circles). The plot $H_{\text{ex}}(d^{\text{MgO}})$ shown by open squares and a solid line, is the same as in Fig. 5. The data (symbols) are fitted with exponentials (lines). $T = 300$ K.

clear picture as the dependence $H_{\text{ex}}(T)$ cannot be distinguished on the background of the strong temperature variations of the magnetocrystalline anisotropy energy²⁴ $K_1(T)$ shown in the inset to Fig. 8. The variation of uniaxial stress-induced anisotropy is also expected but according to the results obtained by Meckenstock *et al.*,²⁵ a resonance line in the saturated epitaxial Fe films is mainly affected by K_1 and film magnetization M . The latter remained almost unchanged within the temperature range 1.4–300 K, as we have verified performing SQUID measurements. Within experimental accuracy the plots $H_r(T)$ obtained for the single Fe film (solid squares) and for the stack [open (H_r^{optic}) and solid (H_r^{acoust}) circles] shown in Fig. 8, are parallel. Therefore the temperature dependence of the coupling strength is not revealed. This makes difficulties for a determination of the temperature behaviour of IC by FMR as well as by SQUID. However, we can obtain some information about the coupling origin by analyzing the temperature dependencies of the

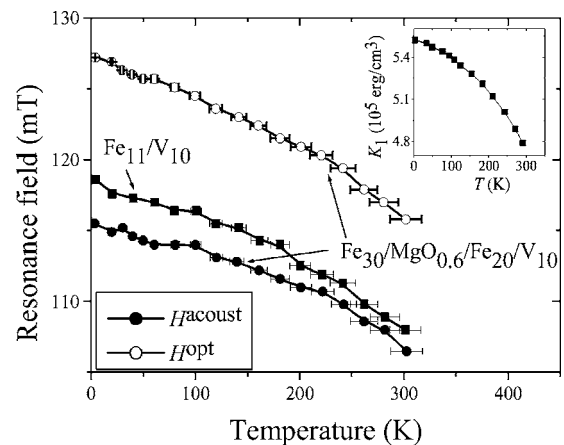


FIG. 8. Temperature dependencies of the parallel resonance fields in $\text{Fe}_{11}/\text{V}_{10}$ (solid squares) and $\text{Fe}_{30}/\text{MgO}_{0.6}/\text{Fe}_{20}/\text{V}_{10}$ (solid and open circles) films. The anisotropy constant K_1 versus temperature (Ref. 24) is shown in the inset.

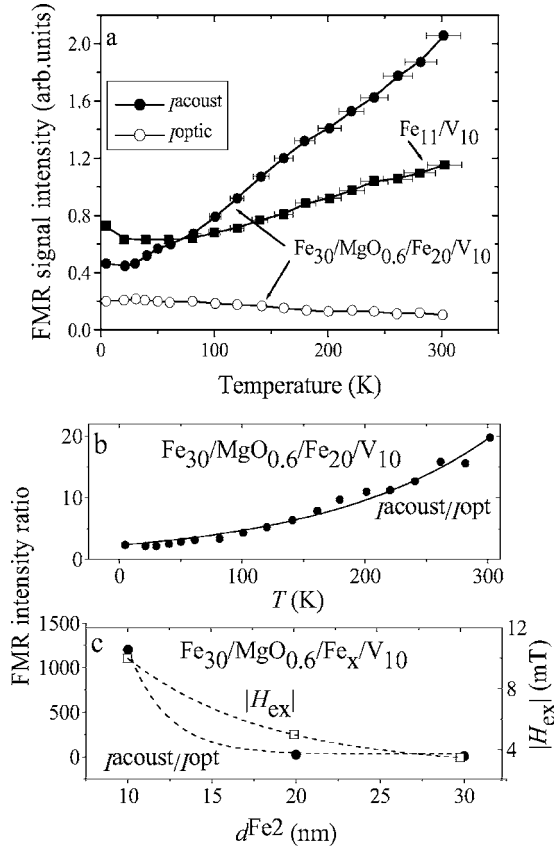


FIG. 9. Temperature dependencies of the FMR signal intensity in $\text{Fe}_{11}/\text{V}_{10}$ (solid squares) and $\text{Fe}_{30}/\text{MgO}_{0.6}/\text{Fe}_{20}/\text{V}_{10}$ (solid and open circles) films (a). The intensity ratio of acoustic and optical peaks as a function of the temperature (b). The FMR intensity ratio (solid circles) and the absolute value of the exchange coupling field (open squares), obtained using SQUID, versus the top Fe layer thickness at $T=300$ K (c). The data (symbols) are fitted with exponentials (lines) (b, c).

resonance signal intensity (I) and FMR linewidth (ΔH) presented in Figs. 9 and 10.

In spite of a slow change of the FMR signal intensity in the single Fe layer below 100 K [Fig. 9(a), solid squares], the acoustic peak (solid circles) keeps decreasing in this temperature range. At the same time, the intensity of the optical peak (open circles) increases. This is clearly seen in Fig. 9(b) where the intensity ratio $I^{\text{acoust}}/I^{\text{optic}}$ is plotted against the temperature. Such behavior for both signals indicates coupling weakening.^{18,19} The latter is confirmed by a correlation between the intensity ratio and the exchange coupling field shown in Fig. 9(c) where both $I^{\text{acoust}}/I^{\text{optic}}$ and $|H_{\text{ex}}|$ are plotted depending on the top Fe layer thickness. The decrease of the interlayer exchange at low temperatures is in agreement with a prediction of the model²³ since the tunneling barrier is higher at lower T .

Figure 10(a) shows that the linewidth in the single Fe layer (ΔH^{Fe}) remains almost unchanged under sample cooling. Generally ΔH is sensitive rather to the anisotropy dispersion than to the K values. The dispersion, and therefore the linewidth, should be larger at interfaces due to imperfections and strains. Inhomogeneous strains tend to relax with

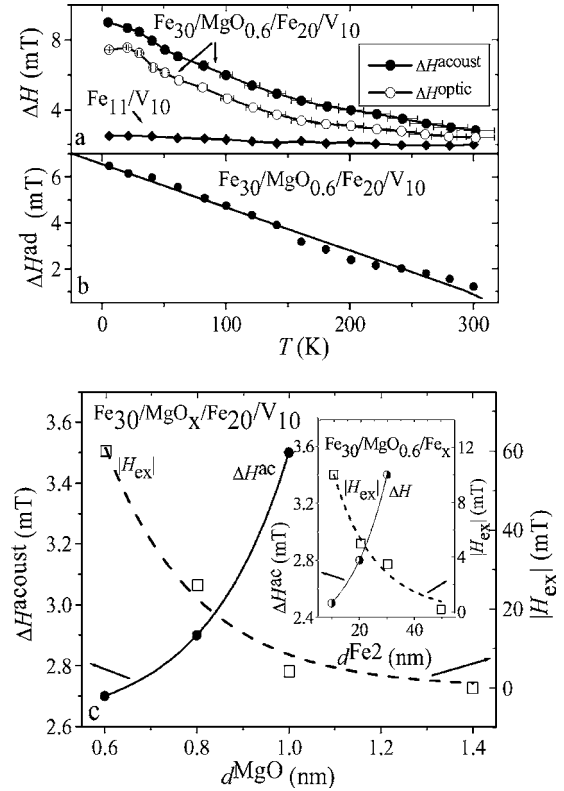


FIG. 10. Temperature dependencies of the parallel FMR linewidth in $\text{Fe}_{11}/\text{V}_{10}$ (solid squares) and $\text{Fe}_{30}/\text{MgO}_{0.6}/\text{Fe}_{20}/\text{V}_{10}$ (solid and open circles) films (a). The additional linewidth $\Delta H^{\text{ad}} = (\Delta H^{\text{Fe}/\text{MgO}/\text{Fe}/\text{V}} - \Delta H^{\text{Fe}/\text{V}})$ as a function of the temperature (b). The parallel FMR linewidth of the acoustic signal (solid circles) and the exchange coupling field $|H_{\text{ex}}|$ (open squares), obtained using SQUID, as functions of the MgO layer thickness at 300 K (c). Room temperature dependencies of both the parallel linewidth and the exchange field on the top Fe layer thickness are shown in the inset. The lines are exponential and linear (ΔH^{ad}) fits.

increasing temperature. However, this does not have a strong influence on the temperature dependence of the linewidth in the iron film [Fig. 10(a)], although two interfaces are available: Fe/MgO (with the substrate) and Fe/V (with the capping layer). Meanwhile in the junction ΔH noticeably increases when the sample is cooled down. Figure 10(b) shows the temperature dependence of the additional (compared to single Fe film) line broadening (ΔH^{ad}) occurring in coupled Fe layers. As can be seen in Fig. 10(c), showing the MgO thickness dependencies of the FMR linewidth and exchange field, line broadening corresponds to decreasing exchange coupling field. A similar behavior of the Fe2 thickness dependencies of ΔH^{acoust} and H_{ex} is demonstrated in the inset. Most probably, resonance line broadening at low temperatures [Figs. 10(a) and 10(b)] means a decrease of the coupling strength. This correlates with the observed temperature behavior of the resonance intensity. However, a mechanism of the inhomogeneous line broadening is actually rather complicated and requires a separate study using FMR at higher frequencies. Such an investigation would allow the observation of an FMR signal in the full range of the angles θ, φ and then quantitative assessments of the coupling strength.

In summary: angular, thickness and temperature dependencies of X-band FMR fields, signal intensities, and linewidths in epitaxial trilayers Fe1/MgO/Fe2/V, as well as in single iron reference films, have been studied. The behavior of the FMR signals agrees with theoretical predictions^{18,19} for the antiferromagnetic layer coupling. The coupling strength decreases with increasing thicknesses of the insulating layer and the iron top layer, as well as under sample cooling. Both the former and the latter are in agreement with the free-electron framework model of the IC coupling⁹ and its temperature dependence.²³ However, in epitaxial Fe/MgO/Fe stacks, a resonance assisted tunneling

mechanism may drive the physics of the AF coupling by spin polarized tunneling beyond the free-electron framework as it has been theoretically considered by Zhuravlev *et al.*¹⁷ Therefore, a realistic interpretation of the temperature dependence of the IC should take into account all these aspects.

ACKNOWLEDGMENTS

We are grateful to the NATO Scientific Council for a support of the research via a CLG grant PST. CLG. 97924. N.A.L. thanks Philip Wigen for useful discussions.

*Corresponding author. Present address: GEMaC, CNRS-UVSQ, 78035 Versailles, France. Electronic address: popova@physique.uvsq.fr

¹*The Physics of Ultra-High-Density Magnetic Recording*. Series in Surface Sciences (Springer-Verlag, Berlin, 2001), p. 350.

²Y. Ando, T. Miyakoshi, M. Oogane, T. Miyazaki, H. Kubota, K. Ando, and S. Yuasa, *Appl. Phys. Lett.* **87**, 142502 (2005).

³S. Yuasa, A. Fukushima, H. Kubota, Y. Suzuki, and K. Ando, *Appl. Phys. Lett.* **89**, 042505 (2006).

⁴D. J. Keavney, E. E. Fullerton, and S. D. Bader, *J. Appl. Phys.* **81**, 795 (1997).

⁵M. Klaua, D. Ullmann, J. Barthel, W. Wulfhchel, J. Kirschner, R. Urban, T. L. Monchesky, A. Enders, J. F. Cochran, and B. Heinrich, *Phys. Rev. B* **64**, 134411 (2001); H. L. Meyerheim, R. Popescu, N. Jedrecy, M. Vedpathak, M. Sauvage-Simkin, R. Pinchaux, B. Heinrich, and J. Kirschner, *ibid.* **65**, 144433 (2002).

⁶E. Popova, J. Faure-Vincent, C. Tiusan, C. Bellouard, M. Hehn, F. Montaigne, M. Alnot, S. Andrieu, A. Schuhl, E. Snoeck, and V. da Costa, *Appl. Phys. Lett.* **81**, 1035 (2002).

⁷J. Faure-Vincent, C. Tiusan, C. Bellouard, E. Popova, M. Hehn, F. Montaigne, and A. Schuhl, *Phys. Rev. Lett.* **89**, 107206 (2002).

⁸C. Martinez Boubeta, J. M. de Teresa, J. L. Costa-Krämer, J. Anguita, D. Serrate, J. I. Arnaud, M. R. Ibarra, A. Cebollada, and F. Briones, *J. Appl. Phys.* **94**, 4006 (2003).

⁹J. C. Slonczewski, *Phys. Rev. B* **39**, 6995 (1989).

¹⁰J. I. Gittleman, Y. Goldstein, and S. Bozowski, *Phys. Rev. B* **5**, 3609 (1972).

¹¹M. Jullière, *Phys. Lett.* **54A**, 225 (1975).

¹²J. M. MacLaren, X. G. Zhang, W. H. Butler, and X. Wang, *Phys. Rev. B* **59**, 5470 (1999).

¹³J. Mathon and A. Umerski, *Phys. Rev. B* **63**, 220403(R) (2001).

¹⁴O. Wunnicke, N. Papanikolaou, R. Zeller, P. H. Dederichs, V. Drchal, and J. Kudrnovsky, *Phys. Rev. B* **65**, 064425 (2002).

¹⁵H. F. Ding, W. Wulfhchel, J. Henk, P. Bruno, and J. Kirschner, *Phys. Rev. Lett.* **90**, 116603 (2003).

¹⁶C. Tiusan, J. Faure-Vincent, C. Bellouard, M. Hehn, E. Jouguelet, and A. Schuhl, *Phys. Rev. Lett.* **93**, 106602 (2004).

¹⁷M. Y. Zhuravlev, E. Y. Tsymbal, and A. V. Vedyayev, *Phys. Rev. Lett.* **94**, 026806 (2005).

¹⁸B. Heinrich and J. F. Cochran, *Adv. Phys.* **42**, 523 (1993).

¹⁹J. Lindner and K. Baberschke, *J. Phys.: Condens. Matter* **15**, S465 (2003).

²⁰G. A. Prinz, G. T. Rado, and J. J. Krebs, *J. Appl. Phys.* **53**, 2087 (1982).

²¹H. Suhl, *Phys. Rev.* **97**, 555 (1955).

²²Yu. V. Goryunov, N. N. Garif'yanov, G. G. Khaliullin, I. A. Garifullin, L. R. Tagirov, F. Schreiber, Th. Mühge, and H. Zabel, *Phys. Rev. B* **52**, 13450 (1995).

²³P. Bruno, *Phys. Rev. B* **49**, 13231 (1994).

²⁴R. M. Bozorth, *Ferromagnetism* (IEEE Press, New York, 1993).

²⁵R. Meckenstock, K. Harms, O. von Geisau, and J. Pelzl, *J. Magn. Magn. Mater.* **148**, 139 (1995).

²⁶J. F. Cochran and V. Kambersky, *J. Magn. Magn. Mater.* **302**, 348 (2006).